Measurements of helical flow of a strong electrolyte with and without a transverse magnetic field

By LAURENCE R. BOEDEKER AND EUGENE E. COVERT
Aerophysics Laboratory, Massachusetts Institute of Technology

(Received 31 December 1962)

This note describes the slow magneto-hydrodynamic flow of hydrochloric acid in a helix. At very low Reynolds number a transverse magnetic field is found to retard the flow in agreement with existing theory and with existing experimental results obtained using mercury. At higher Reynolds numbers where secondary flow in a helix becomes important the transverse magnetic field is found to reduce this secondary flow.

1. Introduction

This report describes an experiment designed to measure the induced effect of a transverse magnetic field on the laminar flow of an electrolyte. Experiments of this nature have been performed earlier† with mercury (Hartmann & Lazarus 1937; Murgatroyd 1953). Electrolytes are interesting, however, because the transport of electricity is a result of migrations of ions of similar masses, unlike the electron conduction of liquid metals. It is of interest to investigate the validity of continuum processes under these different circumstances.

The electrolyte chosen was a solution of hydrochloric acid in water because it has a high conductivity in comparison with electrolytes like salt water and because it is relatively easy to handle. The geometry in which the HCl solution was to flow was selected to give a long interaction length. The configuration that was chosen was a rectangular helical channel that would fit inside a relatively long air core solenoid such that the magnetic field is parallel to the helix axis (figure 1). Thus the helical channel was exposed to a magnetic field that was primarily transverse. The cross-section of the channel was machined on a lathe to insure close tolerances and was nearly square. The helical channel was machined from insulating material which corresponds to the electrical insulating boundary condition.

Helix flow is composed of longitudinal flow and secondary flow. The secondary flow is set up as a result of the radial pressure gradient established by centrifugal action. These two flows are illustrated in figure 1. The initial design of the

† E. J. Williams (1930) has discussed the use of electrolytes in what would now be called magneto-hydrodynamic flow meters. In this application he was interested in flow for which the effects of the body force were negligible. Dr Williams also considered the flow in a helical tube with the magnetic field *normal* to the axis of the helix. This arrangement was used to determine whether or not the secondary flow could be measured. The results did not indicate a secondary velocity.

experiment was based upon the idea that at low enough flow rates the secondary flow in the helix has negligible effects and the flow would correspond to long tube flow.

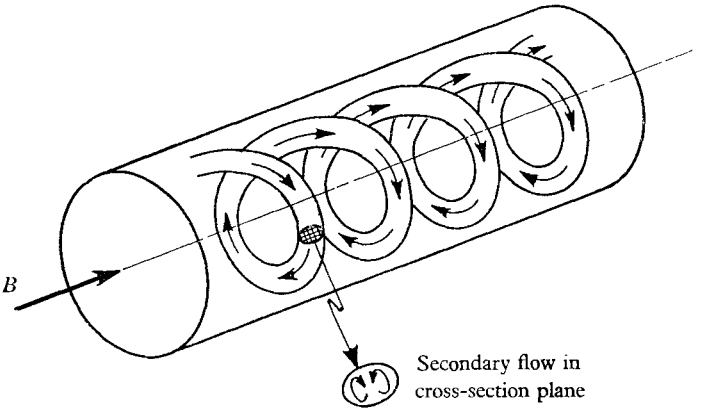

FIGURE 1. Schematic diagram—helical flow in a transverse magnetic field.

The longitudinal flow is nearly perpendicular to the magnetic field. This results in an induced potential perpendicular to both the magnetic field and the flow velocity. The induced potential creates circulating currents which couple with the magnetic field to produced body forces on the fluid tending to flatten out the velocity profile, increase the viscous dissipation and retard the flow. The theory for this type of laminar interaction with longitudinal flow was first worked out for the two-dimensional case by Hartmann & Lazarus (1937) who also obtained experimental results using mercury flowing in a wide variety of channel shapes. Further theoretical and experimental studies using mercury have been carried out by Murgatroyd (1953) and Shercliff (1953). The experimental results with mercury obtained by Hartmann compare well with Shercliff's theory. This theory will be compared with the data from the flow of HCl.

The secondary flow, having velocity components perpendicular to the magnetic field, also tends to set up induced currents which retard this type of motion. Retarding the secondary flow, however, would reduce the viscous dissipation and tend to speed up the flow, an effect which would tend to counteract the longitudinal effect. To date there are apparently no published theoretical treatments on secondary flow interaction with a magnetic field. The experimental results provide a phenomenological description of this type of interaction.

The experiment therefore provides information about the retarding effect of a magnetic field on the longitudinal flow of hydrochloric acid in a helix and about the accelerating effect caused by possible interaction of the magnetic field with the secondary flow. Since the two effects occur simultaneously the net effect of the two is measured.

In designing an experiment in an electrolyte in which there are to be measurable magneto-hydrodynamic interactions it should be realized that while the electrolyte is about 0·1 times as dense as mercury (in which magneto-hydrodynamic interactions have been measured) it has a conductivity that is 2×10^{-4} to 1×10^{-4} times that of mercury.

It is inferred from the momentum equation that interactions will be easy to measure when the magnetic terms are as large as the viscous effect in the physical process. The pressure can be found, approximately, after the velocity is known. A sufficient condition for measurable effects is that the Hartmann number $M = B_0 l(\sigma/\eta)^{\frac{1}{2}}$ must be of order unity while the Reynolds number $\mathrm{Re} = \rho v l/\eta$ is small. Here B_0 is the applied magnetic field strength and l is a characteristic length. Also σ, η, ρ and v are the fluid conductivity, viscosity, density and velocity, respectively. These two requirements together with known approximate fluid property values and a magnetic field strength of from 1 to 5 $\mathrm{Wb/m^2}$ restrict the fluid velocity to very low values.

While this argument is sufficient it is not necessary. It will turn out that interactions can be measured for a less restrictive velocity criterion although flow rates will still require sensitive instrumentation.

It is possible to apply the standard magneto-hydrodynamic approximations (see Shercliff 1953, for example) to the basic equations governing the motion of a conducting fluid in the presence of a magnetic field. This application provides a set of simultaneous equations for the velocity vector $\mathbf{v}$, the magnetic field strength $\mathbf{B}$, and the pressure p. This set of equations can be further simplified since the pressure only occurs in the form of ∇p. This set of equations can be reduced to a simultaneous set of equations for $\mathbf{v}$ and $\mathbf{B}$ by taking the curl of the equation of conservation of momentum. By taking the divergence of the equation of conservation of momentum an equation is obtained that enables the pressure to be found in terms of the velocity and magnetic field after they have been found. If the governing equations are normalized and then solved formally (Morse & Feshback 1953), it turns out that the ratio of the induced magnetic field to the applied magnetic field is proportional to the magnetic Reynolds number, $R_m = \sigma\mu Vl$. Here μ is the fluid magnetic permeability. In this experiment $R_m \leqslant 10^{-7}$. The perturbation pressure is proportional to the dynamic pressure which is approximately 10^{-3} p.s.i.a. for this experiment. Hence it will be difficult to measure changes in pressure and magnetic fields. The primary measurement will be a change in mass flow since measurements can be made for a long time. In dimensional form the governing equations for the fully developed pipe flow are

$$\operatorname{div}\mathbf{v} = 0, \tag{1}$$

$$-\eta \operatorname{curl}\operatorname{curl}\mathbf{v} + \mathbf{J}\times\mathbf{B} - \nabla p = 0, \tag{2}$$

$$\operatorname{curl}\mathbf{B} = \mu\mathbf{J}, \tag{3}$$

where $\mathbf{J}$ is the vector current density and

$$\operatorname{div}\mathbf{B} = 0. \tag{4}$$

The details of the analysis based on these equations may be found in Shercliff's (1953) article. Note that the assumption of fully developed flow causes the inertia terms in equation (2) to be identically zero.†

† The inertia terms are important during the length over which the fully developed pipe flow is established at the entry and at the termination of the channel. This effect can be estimated from either the procedure given by Shercliff (1956) or the procedure given by Lundgren, Atabek & Chang (1961). The starting length or the exit length is approximately $\frac{1}{640}$th the length of the flow along the helical path. Thus the approximation of fully developed pipe flow is applicable to most of the flow.

It is shown by Shercliff (1953) that the average velocity in a rectangular channel of width $2a$ in the direction of the applied magnetic field and of width $2b$ in the other cross-direction is

$$v_0 = \frac{32kb^2}{\pi^4} \sum_{n=0}^{\infty} \frac{1}{(2n+1)^4} \left\{ 1 - \frac{2Nb^2(\cosh N - \cosh M)}{(2n+1)^2 \pi^2 a^2 \sinh N} \right\}, \tag{5}$$

where the pressure drop along the length of the duct is written as $-dp/dz = k\eta$ and

$$N^2 = M^2 + (2n+1)^2 \pi^2 a^2 / b^2.$$

It is easy to show that when the Hartmann number $M < (2n+1)\pi a/b$, the change in average velocity due to the magnetic field is

$$\begin{aligned} \Delta v &= v_0(M, a, b, k) - v_0(0, a, b, k) \\ &\simeq -\frac{32kb^2}{\pi^4} \sum_{n=0}^{\infty} \frac{4b}{\pi a} \frac{\exp\{-(2n+1)\pi a/b\}}{(2n+1)^5} (\cosh M - 1), \end{aligned} \tag{6}$$

and since this series converges rapidly the first term is a good approximation to Δv, i.e.

$$\Delta v \simeq -\frac{32kb^2}{\pi^2} \left[\frac{2b}{\pi a} e^{-\pi a/b} M^2 \right]. \tag{7}$$

An experiment to measure the change in average velocity that is indicated by equation (7) in an electrolytic fluid is discussed below.

2. Experimental technique

In addition to the Hartmann number, $M = (\sigma/\eta)^{\frac{1}{2}} Ba$, another important parameter in this experiment is the secondary flow similarity parameter $K = (d/D)^{\frac{1}{2}} \mathrm{Re}$, where d is a circular pipe diameter and D is the helix diameter. Data obtained by several experimenters (Taylor 1929) using water flowing through a helically wound pipe show that below a value $K \approx 10$, the secondary flow has a negligible contribution to the mass flow-pressure drop relation. Above $K \approx 10$ the secondary flow becomes progressively more important. For a given helix geometry this means that for low enough flow rates the secondary flow will have a negligible contribution to the total flow process. Any interaction of the magnetic field with the secondary flow in this region should thus have negligible effect on the overall flow resistance. However, since the primary or longitudinal effect is independent of Re, the longitudinal effect should be observable in this region.

Dean (1927) has considered the flow in a helix from a theoretical standpoint. He finds that for very low flow rates the flow can be approximately represented by Poiseuille flow. As the flow velocity increases the influence of the centripetal pressure causes a transverse flow in the centre with the return along the edge. This first-order approximation does not contribute to either the mass flow or the pressure drop along the helix. Dean then shows that the second-order terms do contribute to the mass flow and the pressure drop.†

Consequently it seems reasonable to expect that Hartmann type longitudinal interaction can be studied in flows for which the parameter K is less than 10.

† Mr Charles Bartlett, also of this laboratory, has carried out a calculation for flow in square helices and also finds that it is the second-order term that contributes to the pressure drop and mass flow.

Then by increasing the flow rate the form of the interaction can be checked for $K > 10$ as secondary flow becomes more important.

A typical Reynolds number corresponding to $K = 10$ is approximately 30 for channel widths necessary to achieve a significant Hartmann number. This corresponds to low flow rates and introduces flow measurement problems.

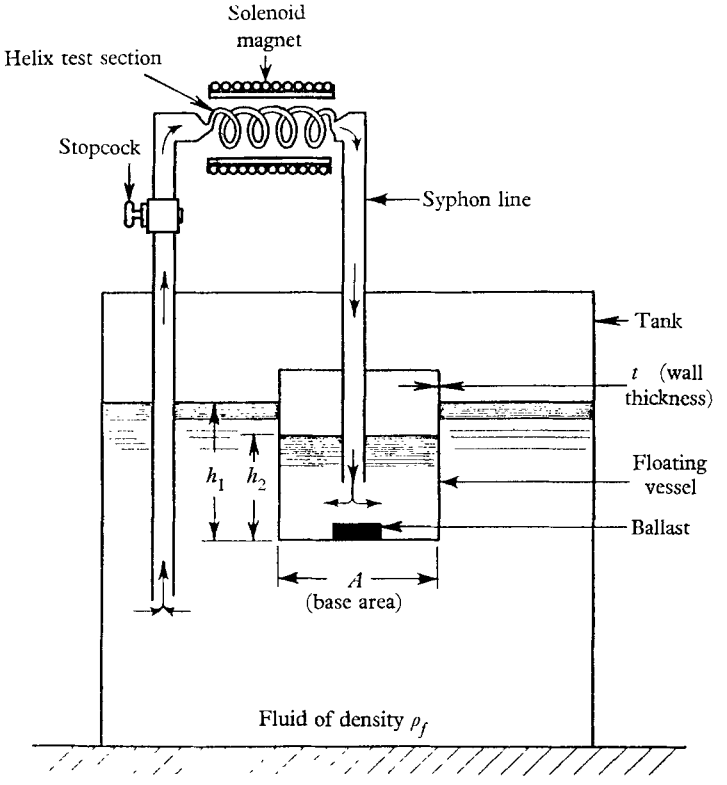

FIGURE 2. Schematic diagram of experimental apparatus.

A buoyancy type device† that maintains a constant pressure head was used to determine the change in mass flow. The buoyancy device will be described below.

3. Experimental apparatus

The principle of the buoyancy Δp controller is illustrated in figure 2. A detailed sketch of the floating vessel is given in figure 3. By making a mass balance it is calculated that the difference in height between the fluid in the tank and the fluid in the floating vessel is

$$h_1 - h_2 = \frac{W_v + W_B}{\rho_f A} - \frac{t(A/\pi)^{\frac{1}{2}}}{A} h_1,$$

where W_v is the floating vessel empty weight, W_B the adjustable ballast weight, t and A the vessel wall thickness and base area, respectively, and ρ_f the fluid

† This device was suggested to the authors by Prof. E. Mollo-Christensen of the Department of Aeronautics and Astronautics, M.I.T

density. Hence, if $t/\sqrt{A} \ll 1$, the device provides a constant head as the floating vessel fills as long as h_1 does not change materially.

The flow is controlled by a large stopcock. The open stopcock and other external syphon tubing are large enough to have negligible resistance compared to the helix test section. Thus any percentage interaction of the magnetic field with the flowing electrolyte will be recorded as an equivalent change in flow rate into the floating vessel while the pressure drop across the helix is maintained essentially constant.

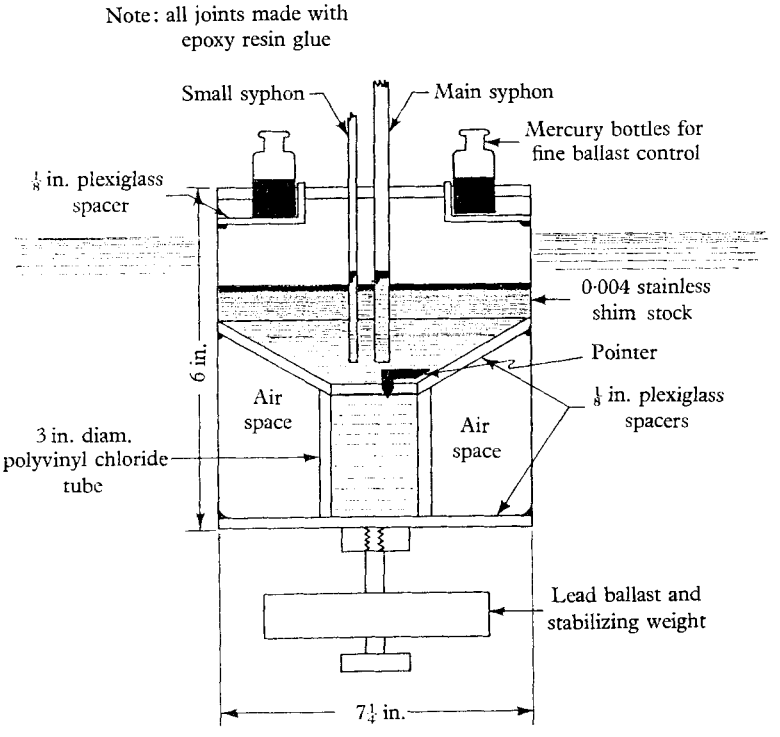

FIGURE 3. Schematic diagram of resultant floating vessel.

A small syphon is used to remove fluid from the floating vessel after a timed run (figure 3). Pressure level control is obtained through adjustment of the weight of small mercury bottles as shown. The walls of the floating vessel are 0·004 in. stainless-steel shim stock sprayed with clear acrylic for acid protection.

The apparatus functions well at the low flow rates desired. It is necessary to keep the walls of the floating vessel and the sloping bottom clean. With clean walls the sinking of the vessel results in a non-wetting meniscus being formed. This type of meniscus give consistent and repeatable results. With a clean bottom the fluid drains more uniformly. Little difficulty is encountered with HCl in keeping the surfaces clean.

Figure 4, plate 1 is a picture of the helix test section. The core of the helix was turned on a lathe from polyvinyl chloride rod stock. Ten turns of a 0·142 by 0·150 in. channel are provided. The channel begins and ends in large diameter bored out sections that lead to glass tube connecting sections. O-ring material

separates the flow channels and prevents the fluid from cutting across channels rather than following the helix. The O-ring at each end keeps the acid from leaking to the outside. A plexiglass tube slips over the core forming the outer wall of the channel and also compressing the O-ring material to make a tight seal.

The instrumentation consists of a pan balance scale to weigh the fluid and a stop-watch to time the flow.

The magnet selected is a $2\frac{1}{8}$ in. air core solenoid magnet at the Massachusetts Institute of Technology Magnet Laboratory. This magnet allows continuous operation with fields of 70,000 G in the centre of the core. Runs of 5 min or more are possible with 90,000 G, depending primarily on the inlet temperature of the coolant water. The power requirement of the magnet with 70,000 G is about one megawatt.

During initial tests with the magnet on, it was noticed that heat dissipation from the magnet was causing a fluid temperature increase of several degrees Fahrenheit. The thermometer arrangement was felt to be too far removed considering the slow flows present. A second set of data was obtained by mounting the bulbs of alcohol thermometers in the inlet and outlet of the helix. This arrangement gave improved temperature data. The useful part of the thermometer scales extended outside the core of the magnet and were easily read. Alcohol thermometers were used to eliminate any possible interaction of the field with a fluid like mercury.

A 10 gallon glazed ceramic jar was used as the tank. A picture of the complete system used to take the first set of data is shown in figure 5, plate 1.

As protection from the acid, polyethylene sheeting was used as much as possible. The entire tank was mounted on cement blocks inside a 55 gallon polyethylene protective drum. The hydrochloric acid itself was transported in 5 gallon polyethylene carboys. Personnel wore protective masks, gloves, and aprons.

The hydrochloric acid used had a specific gravity at 80 °F of about 1·092.

Calibration tests of the system using water and a straight length of $\frac{1}{8}$ in. precision bore glass tubing demonstrated the system's capability for maintaining a constant pressure. The Hagen–Poiseuille relation gave the pressure drop for a measured mass flow at a given value of the ballast weight. In addition the system characteristics using water and the helix test section were found to check well with the existing helix flow data (Taylor 1929).

Surface oscillations of the fluid could possibly affect the pressure head. However, these oscillations induced by generators, air compressors and other machines have had no apparent effect on the flow as no inconsistencies have arisen.

4. Data reduction

Data were taken with a magnet current of 0 and 8000 amp. All data have been referred to a fluid temperature of 26·7 °C (80 °F).†

The Hartmann number was determined to be $M = 3{\cdot}4$ since $\sigma = 88$ mho/m

† Conductivity of the HCl at 18 °C was estimated from the *Handbook of Chemistry and Physics*. An empirical temperature correction was obtained from Harned & Owen (1950). Viscosity and density measurements of the acid were made by Mr Charles W. Haldeman of this laboratory.

at $T = 26{\cdot}7\,^{\circ}\mathrm{C}$, $\eta = 1{\cdot}12 \times 10^{-3}\,\mathrm{kg/m\ sec}$ at $T = 26{\cdot}7\,^{\circ}\mathrm{C}$, $B = 6{\cdot}8\,\mathrm{Wb/m^2}$, and $a = 0{\cdot}071\,\mathrm{in.} = 1{\cdot}80 \times 10^{-3}\,\mathrm{m}$. The value $B = 68{,}000\,\mathrm{G}$ is an average. The actual field varied from 72,000 G at the centre of the helix to about 63,000 at the edge. An uncertainty is possible of $\pm 1000\,\mathrm{G}$ in B or about $\pm 1{\cdot}5\,\%$ due to uncertainties in the appropriate value of B to choose. Together with an estimated uncertainty of 2 % in the conductivity and 1 % in viscosity the overall Hartmann number uncertainty is estimated at $\pm 3\,\%$. This makes $M = 3{\cdot}4 \pm 0{\cdot}1$.

The uncertainty in M is estimated from Shercliff's theory to contribute a 1 % uncertainty in the theoretical percentage interaction.

The measured data were taken in the form of changes in mass, time, and temperature. Data reduction was complicated by significant temperature changes of the fluid in the helix caused by heat dissipation from the magnet. For these data the alcohol thermometers provided a time history of helix inlet and outlet temperature.

The mass flow is a function of the fluid kinematic viscosity ν and ν is a function of temperature. Using the average of the inlet and outlet temperatures at any instant, a time history of average kinematic viscosity $\bar{\nu}$ was obtained. From this an overall time weighted average $\bar{\bar{\nu}}$ was calculated for each run. The experimental value of mass flow for the run was then corrected to $26{\cdot}7\,^{\circ}\mathrm{C}$ ($80\,^{\circ}\mathrm{F}$) the reference temperature chosen. The Hartmann number changes slightly when the data are referred to $26{\cdot}7\,^{\circ}\mathrm{C}$. A small mass flow correction was applied to account for the effect.

It was desired to change the fine ballast scale to one involving the actual pressure drop. To do this the system was calibrated with the HCl solution using $\frac{1}{8}$ in. precision bore glass tubing in the manner discussed in the previous section. In applying this calibration to the ballast scale, two other corrections were applied. One allowed for the finite resistance of the large tubing in the syphon line and the other accounted for the small change in pressure head maintained by the constant pressure device during a run. The net effect of these two was to reduce the calibration constant by 1·7 %. The resultant calibration constant was determined to be

$$\frac{\Delta p}{W_B} = 315\,\frac{\mathrm{Newton/m^2}}{\mathrm{kg}}.$$

The resultant scale was divided by the length of the helix channel to give the final results in terms of dp/dz.

The data in terms of ballast weight and mass flow corrected to $26{\cdot}7\,^{\circ}\mathrm{C}$ are plotted in figure 6. After shifting the origin to the zero flow point on figure 6 the appropriate calibration constant was applied to the ballast scale and the final results in terms of dp/dz are shown in figure 7. Some points at $W_B = 0{\cdot}27\,\mathrm{kg}$ on figure 6 are not shown on figure 7. These points were found to be inconsistent with the other data and are thought to be traceable to an error in weighing the mercury bottles used for fine ballast. These weights were subsequently changed before the inconsistency was detected, however, thus not permitting a recheck.

The initial data was subsequently used to determine the initial zero field slope, two points at $W_B = 0{\cdot}018$ and $0{\cdot}27\,\mathrm{kg}$ being used. One of these points was taken before and one well after the magnet was used. Hence the temperature would

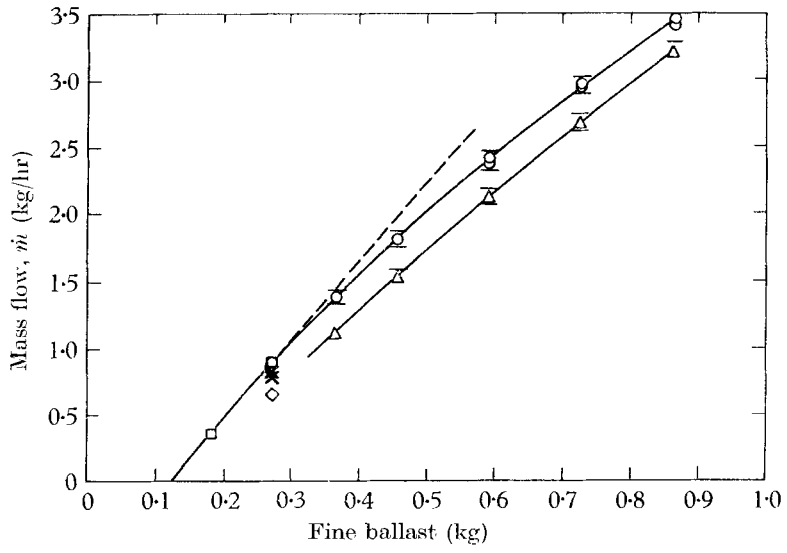

FIGURE 6. Mass flow *vs* ballast. The various points are: □, From initial data, $M = 0$; ○, final data, $M = 0$; △, final data, $M = 3{\cdot}4$; ×, inconsistent points, $B = 0$; ◇, inconsistent points, $B = 68{,}000$ G. The vertical limits indicate the 2 % scatter band.

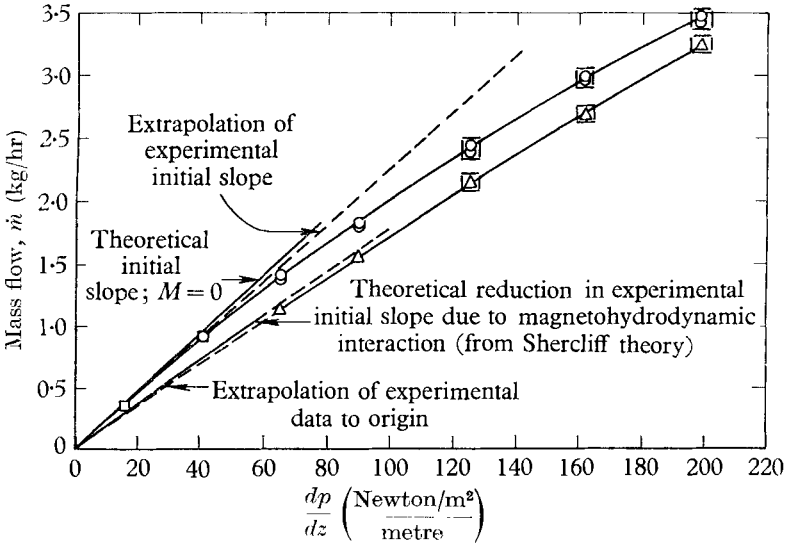

FIGURE 7. Mass flow *vs* pressure gradient. The symbols are as in figure 6, with the 2 % horizontal limits for the uncertainty in dp/dz.

be expected to remain relatively constant and the thermometer readings were taken as being the helix temperature. The data indicated that $W_B = 0{\cdot}27$ lb. was about the limit of the linear region.

An estimated scatter band for mass flow of 2 % is indicated about the points in figures 6 and 7. This is associated with errors in adding and removing fluid to

the floating vessel and with inaccuracies in measuring temperatures. By starting with a known amount of fluid, adding it to the vessel, removing it and rechecking its mass it was determined that the mass could be duplicated to within at most ± 2 g. During data taking, between 200 and 400 g of HCl was allowed to flow, the running time being cut down at the higher flow rates. Thus, the process of adding and removing fluid could be expected to form a 0·5–1·0 % scatter band. Because of inaccuracies in reading the thermometers and to possible non-linearities in the temperature distribution along the helical flow path it is thought that a $\pm 0{\cdot}5$ °C temperature inaccuracy should be included. This contributes about a ± 1 % scatter band in applying the kinematic-viscosity correction to the data and about $\pm \frac{1}{4}$ % in applying the Hartmann-number correction. Thus a scatter band of from $\pm 1{\cdot}75$ to $\pm 2{\cdot}25$ % would seem appropriate, 2 % being indicated on the data plots.

An experimentally determined scatter band was not feasible due to the length of time involved in taking each point. Each point was repeated at least twice, however. Those points that appear as only one actually represent two almost indentical trials. All points are seen to lie within the 2 % scatter band.

The other measured quantities, time and fine ballast, were all determinable to well below 1 % and have not been included in the scatter band. Because of similar uncertainties in the calibration process a 2 % scatter band has been applied to the dp/dz values on figure 7.

5. Discussion

The data in figures 6 and 7 shows the linear region of the $M = 0$ curve at low flow rates and the bending downwards of the curve as secondary flow in the helix becomes important. Insufficient data were obtained to determine the $M = 3{\cdot}4$ curve in the low-flow region. The higher points obtained for $M = 3{\cdot}4$ indicate an extension of the linear region into the normally secondary-flow region. This indicates a damping of the secondary flow by the magnetic field. A less pronounced curving downwards then takes place and the $M = 3{\cdot}4$ curve approaches closer to the $M = 0$ curve. With the present apparatus an extension of the curves to higher flow rates to determine whether they approach each other asymptotically or actually cross was not possible. There are theoretical considerations which indicate that the $M =$ const. curves approach the $M = 0$ curve asymptotically, but do not cross it. The discussion of this point will be deferred until more evidence is available.

The $M = 3{\cdot}4$ curve has been extrapolated linearly to the origin, clearly consistent with the data and with the expected phenomenological behaviour. An experimental investigation of this region is possible but time limitations prevented its being done.

Theoretical values of the initial slopes of pressure-drop–mass-flow curves for the helix have been calculated for the cases of $M = 0$ and $M = 3{\cdot}4$. The theory developed by Shercliff (1953) for rectangular cross-sections has been used. Shercliff's theory agrees very well with the data of Hartmann who used mercury as the conducting fluid (1937).

The $M = 0$ theoretical curve is plotted on figure 7. Its slope is close to the experimental value, being about 4 % higher. The theoretical ratio of

$$\frac{(\dot{m})_{M=0}}{(\dot{m})_{M=3\cdot4}} \text{ at constant } \frac{dp}{dz}$$

has been applied to the experimental $M = 0$ initial slope. This is felt to be a more valid test of the data than plotting the theoretical $M = 3{\cdot}4$ curve directly. The initial slope ratios are directly obtainable from the data. Comparing the absolute value of the theoretical and experimental slopes involves the additional uncertainties of the indirect calibration process.

Shercliff's theory gives with $a/b = 0{\cdot}947$

$$\left(\frac{\dot{m}_{M=3\cdot4}}{\dot{m}_{M=0}}\right)_{\text{theory}} = 0{\cdot}798 \text{ at constant } \frac{dp}{dz}.$$

This fraction has been applied to the experimental $M = 0$ initial slope and the resultant line is indicated in figure 7. The experimental interaction is seen to be slightly greater than the theoretical, being about

$$\left(\frac{\dot{m}_{M=3\cdot4}}{\dot{m}_{M=0}}\right)_{\text{exp.}} = 0{\cdot}77 \text{ at constant } \frac{dp}{dz}.$$

The difference between these latter two values is about 4 %. This agreement between theory and experiment is felt to be adequate, while the 2 % uncertainty band about the experimental points, plus the uncertainty in the Hartmann number could be sufficient to explain the 4 % difference between the experimental and theoretical magneto-hydrodynamic interaction. Since there is a 4 % difference between theory and experiment for the absolute value of the $M = 0$ initial slopes, which is outside the 2 % uncertainty band, a direct calibration of the system would seem desirable to eliminate the possibility of additional unaccountable systematic errors in calibration.

The general agreement between these experimental results and Shercliff's theory indicates that the flow of liquid metals is similar to the flow of electrolytic fluid. The differences in constituents is accounted for by the transport properties. As a consequence of the experimental results obtained here, when interpreted with Hartmann's results and Shercliff's theoretical predictions, it is concluded that the one-fluid model of incompressible magneto-hydrodynamic flow is valid in the absence of large gradients.

As stated previously there is apparently no theory at present that will describe the damping of secondary flow by a magnetic field that is indicated by the data.

No data were taken at other magnetic field strengths. Thus no information on interaction versus Hartmann number has been obtained. Hartmann numbers higher than $M = 3{\cdot}4$ are not possible with the present helix. A magnet current of 8000 amp is the maximum attainable for the long-duration testing that is necessary. An increased flow channel dimension would be necessary for increased M, but this would require all other components of the system to be increased in size to accommodate the increased mass flows and a complete rebuilding of equipment would be required. Hartmann numbers lower than $M = 3{\cdot}4$ would be

possible of course, but the interaction would become very small making cross-plotting difficult.

A study of the data of figures 6 and 7 indicates that the effect of a transverse magnetic field on the flow of hydrochloric acid in a helix consists of two parts: (*a*) a reduction in mass flow for a fixed pressure gradient, and (*b*) a reduction in the secondary losses in the helix.

This study was supported by the Office of Scientific Research (USAF) under contract AF 49(638–900). The authors would like to acknowledge the enthusiastic support of Mr I. R. Schwartz, now of NASA, in the early stages of the work.

REFERENCES

DEAN, W. R. 1927 *Phil. Mag.* **4**, 208.

HARNED, H. S. & OWEN, B. B. 1950 *The Physical Chemistry of Electrolytic Solutions.* New York: Reinhold.

HARTMANN, J. & LAZARUS, F. 1937 *Mat.-Fys. Medd. Danske Vid. Selsk.* **15**, 7.

LUNDGREN, T. S., ATABEK, B. H. & CHANG, C. C. 1961 *Phys. Fluids*, **4**, 1006.

MORSE, D. M. & FESHBACK, H. 1953 *Methods of Theoretical Physics.* New York: McGraw Hill.

MURGATROYD, W. 1953 *Phil. Mag.* (7), **44**, 1348.

SHERCLIFF, J. A. 1953 *Proc. Camb. Phil. Soc.* **49**, 136.

SHERCLIFF, J. A. 1956 *J. Fluid Mech.* **6**, 644.

TAYLOR, G. I. 1929 *Proc. Roy. Soc.* A, **124**, 243.

WILLIAMS, E. J. 1930 *Proc. Phys. Soc.* **42**, 466.

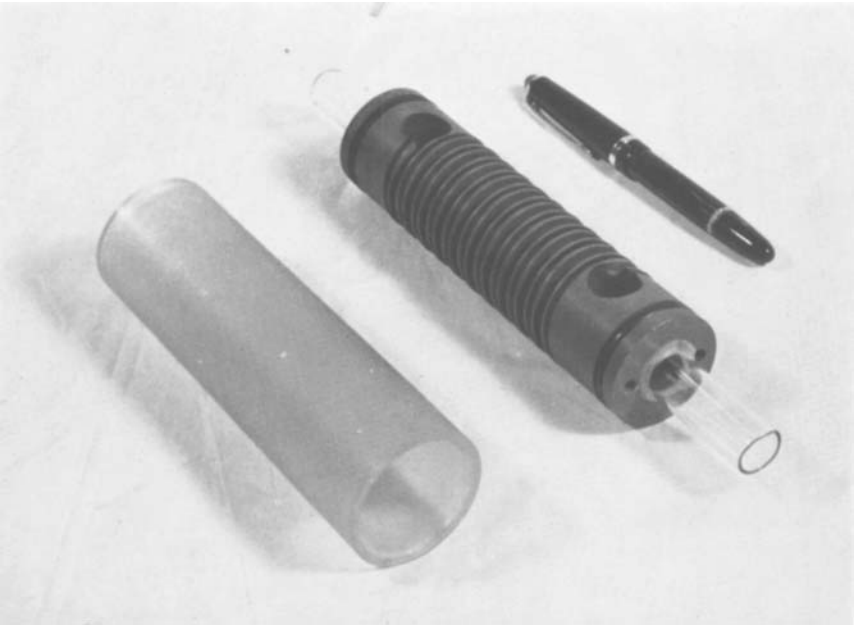

FIGURE 4. Picture of helix test section.

FIGURE 5. System set up in magnet.